チル化を指標として，ゲノム上の脂肪細胞・前駆脂肪細胞に濃縮されるエンハンサー領域を同定し，モチーフ解析を組み合せることで，PLZF と SRF という2つの負のレギュレーターを同定した．

脂肪細胞特異的オープンクロマチン領域解析（FAIRE-seq）

ヒトゲノム計画によってゲノム上の DNA 配列が決定され，2万～2万5千の遺伝子が存在することが明らかにされた[2]．ポストゲノム時代の大きな課題の1つは，ゲノム上の遺伝子を制御する“制御領域”を同定することである．古典的には DNaseI に対するクロマチンの感受性を用いた DNaseI hypersensitivity 法が用いられるが，これとシークエンサーを組み合わせた DNase-seq や[27]，H3K4 のメチル化，アセチル化，p300 の結合などを指標とした ChIP-seq などを用いた，組織特異的なエンハンサー領域の同定が報告されている[28][29]．Folmalidehyde-assisted isolation of regulatory elements（FAIRE）は Lieb らにより開発された方法で，DNaseI hypersensitivity 法と同様に，ヒストン（ヌクレオソーム）フリーのゲノム領域（＝オープンクロマチン領域）を検出する[30]．原理はゲノムのホルマリン固定，断片化に続いてフェノールクロロホルム抽出を行うことによって，オープンクロマチン領域にあるタンパク（ヒストン）に架橋されなかったゲノム DNA 断片が濃縮される（図4）．1つの有用なアプリケーションとして，FAIRE と次世代シークエンスを組み合わせた FAIRE-seq により同定された膵島特異的オープンクロマチン領域をガイドとして，ゲノムワイド関連解析（GWAS）で認められた疾患感受性領域の中の causal SNP が同定された成功例が挙げられる[31]．

我々は FAIRE-seq を用いて，脂肪細胞 3T3-L1 のゲノム上のオープンクロマチン領域を解析した（図5）．37,781ヵ所のオープンクロマチン領域のうち 28％ はプロモーター領域，残りは非プロモーター領域に存在した．プロモーター領域の FAIRE は H3K4me3 や H3K27ac（アセチル化）のプロモーター型ヒストン修飾で，非プロモーター領域の FAIRE は H3K4me1＋，H3K27ac＋，H3K4me3－のエンハンサー型ヒストン修飾を示した．興味深いことに，脂肪細胞分

図4　FAIRE によるオープンクロマチン領域の検出

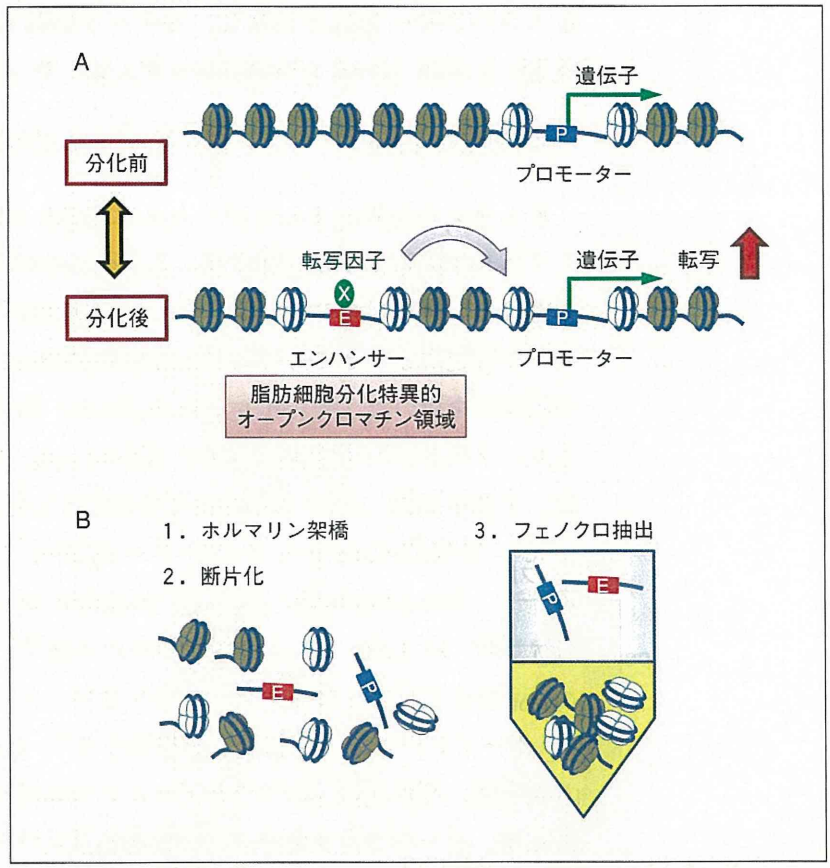

A：エンハンサーやプロモーターなどの制御領域はオープンクロマチン構造をとる．分化前後で変化するオープンクロマチン領域には分化を制御するエンハンサー領域が含まれる．
B：FAIRE の原理

化前後でプロモーター FAIRE は変化しないのに対し，非プロモーター FAIRE はダイナミックに変化していた．脂肪細胞分化に伴ってオープンクロマチンを呈する領域は脂肪細胞分化で制御される遺伝子，また脂肪分化や糖脂質代謝にかかわる遺伝子の近傍に濃縮しており，その数が多ければ多いほど遺伝子の転写が制御される傾向にあった．これらのことから，脂肪細胞特異的な非プロモーター FAIRE 領域が，細胞特異的な制御に重要な役割を果たすことが示された．またそれらの 45.3％，11.7％ は，ChIP-seq で同定された PPARγ および C/EBPα 結合領域とオーバーラップしており，これらが主要な脂肪

図5　*Klf15* 遺伝子領域の FAIRE シグナル

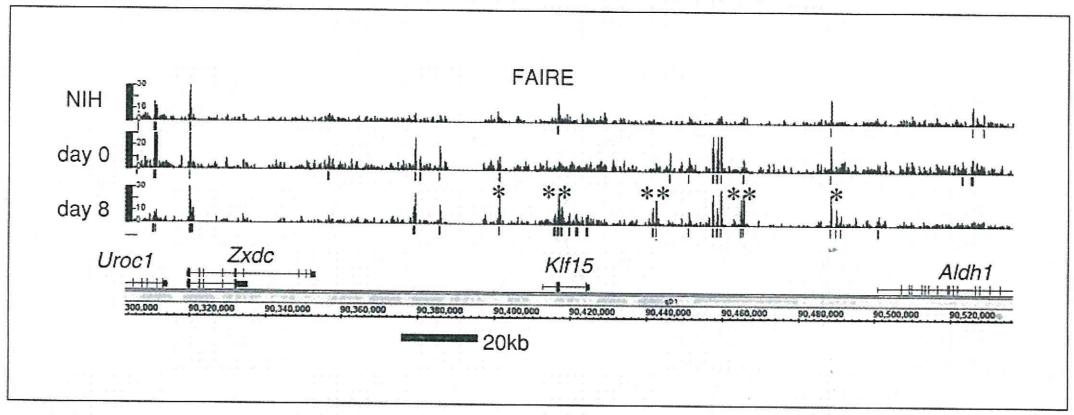

上段から NIH-3T3，3T3-L1 day 0，3T3-L1 day 8．下線は有意なピーク（FDR＜10^{-4}）．＊は脂肪細胞特異的なオープンクロマチン領域．

図6　脂肪細胞特異的オープンクロマチン領域に濃縮される転写因子の結合モチーフ解析（Transfac データベース Release 2010.4）

Motif	Name	Corrected P-value	Enrich-ment Ratio (Ad / pAd)	Logo
M00193	NF-1	7.9E-27	1.60	
M01196	CTF1	5.1E-22	1.55	
M01100	LRF	2.6E-20	1.65	
M00528	PPAR	2.7E-12	2.14	
M01728	EAR2	1.2E-09	1.47	
M01031	HNF4 (PPAR)	3.8E-08	2.06	
M01772	C / EBP	1.7E-07	2.69	
M00109	C / EBPβ	3.1E-07	1.51	

PPAR や C / EBP のほかに NFI（CTF1）のモチーフが濃縮している．

図7　3T3-L1 脂肪細胞分化における NFIA，NFIB のノックダウンの効果

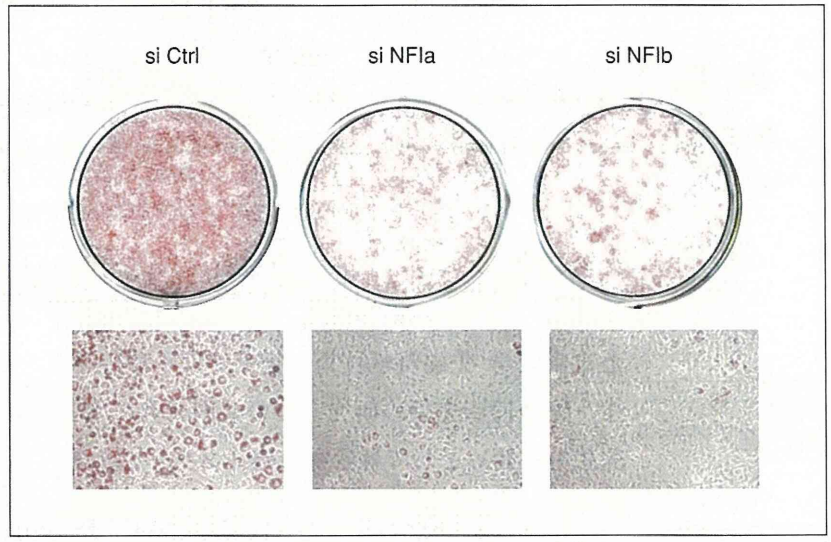

細胞分化制御因子であることに合致した．

FAIRE-seq は特定の転写因子に対する ChIP-seq と異なり，“制御領域”をバイアスなく検出する．オープンクロマチン領域の FAIRE-seq による検出とバイオインフォルマティクスによるモチーフ解析を組み合せることは，新たな制御因子の同定に有用であると考えられる．3T3-L1 の分化の前後で変化する分化特異的なオープンクロマチン領域に濃縮されるモチーフ解析を施行したところ，既知のマスターレギュレーターである PPARγ と C/EBP の結合モチーフに加えて，脂肪細胞での機能が知られていない転写因子の結合モチーフが含まれていた（図6）．これらのモチーフの1つに結合する NFI 転写因子についてその機能を検討した．NFI は NFIA，NFIB，NFIC，NFIX の4種類の遺伝子から成るファミリーであるが，中でも NFIA，NFIB は分化でその発現が上昇し，組織パネルにおいても脂肪組織に発現が多くみられた．3T3-L1 細胞で NFIA と NFIB に対する short interfering RNA（siRNA）によるノックダウンを行うと，PPARγ，C/EBPα，その下流の aP2 などの遺伝子の分化依存な誘導が抑制され，oil red O 染色でトリグリセリド蓄積の抑制がみられ，NFIA，NFIB が脂肪細胞分化に生理的な役割を果たしていることが示唆された（図7）．

おわりに

近年のゲノムサイエンス分野における最も大きなブレークスルーである次世代シークエンサーを利用したエピゲノム・転写因子研究について，脂肪細胞分化における新しい知見をまとめた．今後，脂肪細胞分化のみならず，広くメタボリックシンドロームに関連した病態生理においてゲノムワイド解析が，既存の研究手法とは全く異なる新たな知見を与えてくれるものと期待される．最後に，本研究は門脇研究室と東京大学 先端科学技術研究センターの油谷浩幸先生，酒井寿郎先生，児玉龍彦先生の研究室との共同研究により得られた成果であり，先生方を始めとして各研究室のメンバーにこの場を借りて深謝いたします．

文　献

1) Collins F: Has the revolution arrived ?　Nature 464: 674–675, 2010.
2) Lander E S, et al: Initial sequencing and analysis of the human genome. Nature 409: 860–921, 2001.
3) Wheeler D A, et al: The complete genome of an individual by massively parallel DNA sequencing.　Nature 452: 872–876, 2008.
4) Service R F: Gene sequencing. The race for the $1000 genome.　Science 311: 1544–1546, 2006.
5) Tontonoz P, et al: Stimulation of adipogenesis in fibroblasts by PPAR gamma 2, a lipid–activated transcription factor.　Cell 79: 1147–1156, 1994.
6) Rosen E D, et al: PPAR gamma is required for the differentiation of adipose tissue in vivo and in vitro.　Mol Cell 4: 611–617, 1999.
7) Kubota N, et al: PPAR gamma mediates high–fat diet–induced adipocyte hypertrophy and insulin resistance.　Mol Cell 4: 597–609, 1999.
8) Barak Y, et al: PPAR gamma is required for placental, cardiac, and adipose tissue development.　Mol Cell 4: 585–595, 1999.
9) Tontonoz P, et al: Fat and beyond: the diverse biology of PPARgamma. Annu Rev Biochem 77: 289–312, 2008.
10) Nielsen R, et al: Genome–wide profiling of PPARgamma: RXR and RNA polymerase II occupancy reveals temporal activation of distinct metabolic pathways and changes in RXR dimer composition during adipogenesis. Genes Dev 22: 2953–2967, 2008.
11) Lefterova M I, et al: PPARgamma and C/EBP factors orchestrate adipocyte biology via adjacent binding on a genome–wide scale.　Genes Dev 22: 2941–2952, 2008.

12) Nakachi Y, et al: Identification of novel PPARgamma target genes by integrated analysis of ChIP-on-chip and microarray expression data during adipocyte differentiation. Biochem Biophys Res Commun 372: 362-366, 2008.
13) Wakabayashi K, et al: The peroxisome proliferator-activated receptor gamma/retinoid X receptor alpha heterodimer targets the histone modification enzyme PR-Set7/Setd8 gene and regulates adipogenesis through a positive feedback loop. Mol Cell Biol 29: 3544-3555, 2009.
14) Hamza M S, et al: De-novo identification of PPARgamma/RXR binding sites and direct targets during adipogenesis. PLoS One 4: e4907, 2009.
15) Steger D J, et al: Propagation of adipogenic signals through an epigenomic transition state. Genes Dev 24: 1035-1044, 2010.
16) Lefterova M I, et al: Cell-specific determinants of peroxisome proliferator-activated receptor gamma function in adipocytes and macrophages. Mol Cell Biol 30: 2078-2089, 2010.
17) Mikkelsen T S, et al: Comparative epigenomic analysis of murine and human adipogenesis. Cell 143: 156-169, 2010.
18) Okamura M, et al: COUP-TFII acts downstream of Wnt/beta-catenin signal to silence PPARgamma gene expression and repress adipogenesis. Proc Natl Acad Sci USA 106: 5819-5824, 2009.
19) Cho Y W, et al: Histone methylation regulator PTIP is required for PPARgamma and C/EBPalpha expression and adipogenesis. Cell Metab 10: 27-39, 2009.
20) Wang L, et al: Histone H3K27 methyltransferase Ezh2 represses Wnt genes to facilitate adipogenesis. Proc Natl Acad Sci USA 107: 7317-7322, 2010.
21) Lee J, et al: Targeted inactivation of MLL3 histone H3-Lys-4 methyltransferase activity in the mouse reveals vital roles for MLL3 in adipogenesis. Proc Natl Acad Sci USA 105: 19229-19234, 2008.
22) Tateishi K, et al: Role of Jhdm2a in regulating metabolic gene expression and obesity resistance. Nature 458: 757-761, 2009.
23) Inagaki T, et al: Obesity and metabolic syndrome in histone demethylase JHDM2a-deficient mice. Genes Cells 14: 991-1001, 2009.
24) Takada I, et al: A histone lysine methyltransferase activated by non-canonical Wnt signalling suppresses PPAR-gamma transactivation. Nat Cell Biol 9: 1273-1285, 2007.
25) Carroll J S, et al: Chromosome-wide mapping of estrogen receptor binding reveals long-range regulation requiring the forkhead protein FoxA1. Cell 122: 33-43, 2005.
26) Siersbæk R, et al: Extensive chromatin remodelling and establishment of transcription factor 'hotspots' during early adipogenesis. Embo J 30: 1459-1472, 2011.
27) Song L, et al: DNase-seq: a high-resolution technique for mapping active gene regulatory elements across the genome from mammalian cells. Cold

Spring Harb Protoc pdb prot5384, 2010.
28) Wang Z, et al: Combinatorial patterns of histone acetylations and methylations in the human genome. Nat Genet 40: 897–903, 2008.
29) Heintzman N D, et al: Distinct and predictive chromatin signatures of transcriptional promoters and enhancers in the human genome. Nat Genet 39: 311–318, 2007.
30) Giresi P G, et al: Isolation of active regulatory elements from eukaryotic chromatin using FAIRE (Formaldehyde Assisted Isolation of Regulatory Elements). Methods 48: 233–239, 2009.
31) Gaulton K J, et al: A map of open chromatin in human pancreatic islets. Nat Genet 42: 255–259, 2010.
32) American Association for Cancer Research Human Epigenome Task Force; European Union, Network of Excellence, Scientific Advisory Board.: Moving AHEAD with an international human epigenome project. Nature 454: 711–715, 2008.

Epigenetic Regulation of Adipocyte Differentiation

Hironori Waki[1,2], Masahiro Nakamura[2], Toshimasa Yamauchi[2], Takashi Kadowaki[2]

[1] Functional Regulation of Adipocytes
[2] Department of Diabetes and Metabolic Diseases, Graduate School of Medicine, the University of Tokyo

● 成因と病態：遺伝子・病態・標的分子の面から

褐色脂肪細胞とエネルギー消費

天使大学大学院 看護栄養学研究科 教授
斉藤昌之

要旨

調節性熱産生の特異的部位である褐色脂肪は，交感神経性の刺激によって活性化され，全身エネルギー消費や体温，体脂肪量の調節に寄与している．ヒト褐色脂肪は加齢とともに減少し，同時に肥満が進展するが，褐色脂肪を維持する者は中高年になっても肥満しない．今後，褐色脂肪を増量・活性化する内的・外的要因が解明されれば，肥満制御への手掛かりとなろう．

はじめに

メタボリックシンドロームの基盤に肥満，特に内臓脂肪型肥満があることは周知の事実である．この内臓脂肪は白色脂肪組織を指しているが，ヒトを含めてほ乳動物にはもう1種類の脂肪組織，褐色脂肪が存在する．褐色脂肪と白色脂肪とは存在部位や形態が異なっているが，最も際立った違いはその生理的役割である．白色脂肪は余剰のエネルギーをトリグリセリド（TG）として細胞内に蓄え，必要に応じて脂肪酸として細胞外に放出し全身に供給する「エネルギーの貯蔵と放出」の部位であるが，褐色脂肪は脂肪酸をそれ自身で酸化分解して熱を産生する「エネルギーの消費と散逸」の部位である．褐色脂肪は冬眠動物や小型げっ歯類での発熱組織として古くから知られていたが，脂肪

キーワード：褐色脂肪組織，交感神経，UCP，FDG-PET，肥満

doi:10.1016/j.jmb.2011.06.028 J. Mol. Biol. (2011) 411, 986–998

Contents lists available at www.sciencedirect.com

Journal of Molecular Biology

journal homepage: http://ees.elsevier.com.jmb

Crystal Structure of the Eukaryotic Light-Driven Proton-Pumping Rhodopsin, *Acetabularia* Rhodopsin II, from Marine Alga

Takashi Wada[1], Kazumi Shimono[1,2], Takashi Kikukawa[3], Masakatsu Hato[1], Naoko Shinya[1], So Young Kim[4], Tomomi Kimura-Someya[1], Mikako Shirouzu[1], Jun Tamogami[2,3], Seiji Miyauchi[2], Kwang-Hwan Jung[4], Naoki Kamo[2]* and Shigeyuki Yokoyama[1,5]*

[1]*RIKEN Systems and Structural Biology Center, Yokohama 230-0045, Japan*
[2]*College of Pharmaceutical Sciences, Matsuyama University, Matsuyama 790-8578, Japan*
[3]*Faculty of Life Science, Hokkaido University, Sapporo 060-0810, Japan*
[4]*Department of Life Science and Institute of Biological Interfaces, Sogang University, Seoul 121-742, Korea*
[5]*Department of Biophysics and Biochemistry, Graduate School of Science, The University of Tokyo, Tokyo 113-0033, Japan*

Received 6 June 2011;
accepted 15 June 2011
Available online
25 June 2011

Edited by R. Huber

Keywords:
microbial rhodopsin;
cell-free protein synthesis;
lipidic mesophase;
proton-releasing residues;
proton transfer

Acetabularia rhodopsin (AR) is a rhodopsin from the marine plant *Acetabularia acetabulum*. The opsin-encoding gene from *A. acetabulum*, ARII, was cloned and found to be novel but homologous to that reported previously. ARII is a light-driven proton pump, as demonstrated by the existence of a photo-induced current through *Xenopus* oocytes expressing ARII. The photochemical reaction of ARII prepared by cell-free protein synthesis was similar to that of bacteriorhodopsin (BR), except for the lack of light–dark adaptation and the different proton release and uptake sequence. The crystal structure determined at 3.2 Å resolution is the first structure of a eukaryotic member of the microbial rhodopsin family. The structure of ARII is similar to that of BR. From the cytoplasmic side to the extracellular side of the proton transfer pathway in ARII, Asp92, a Schiff base, Asp207, Asp81, Arg78, Glu199, and Ser189 are arranged in positions similar to those of the corresponding residues directly involved in proton transfer by BR. The side-chain carboxyl group of Asp92 appears to interact with the sulfhydryl group of Cys218, which is unique to ARII and corresponds to Leu223 of BR and to Asp217 of *Anabaena* sensory rhodopsin. The orientation of the Arg78 side chain is opposite to the corresponding Arg82 of BR. The putative absence of water molecules around Glu199 and Arg78 may disrupt the formation of the low-barrier hydrogen bond at Glu199, resulting in the "late proton release".

*Corresponding authors. N. Kamo is to be contacted at: College of Pharmaceutical Sciences, Matsuyama University, 4-2 Bunkyo-cho, Matsuyama, Ehime 790-8578, Japan; S. Yokoyama, RIKEN Systems and Structural Biology Center, 1-7-22 Suehiro-cho, Tsurumi, Yokohama, 230-0045, Japan. E-mail addresses: nkamo@cc.matsuyama-u.ac.jp; yokoyama@biochem.s.u-tokyo.ac.jp.

Abbreviations used: AR, *Acetabularia* rhodopsin; ASR, *Anabaena* sensory rhodopsin; BR, bacteriorhodopsin; ITO, indium tin oxide; NpHR, halorhodopsin from *Natronomonas pharaonis*; NpSRII, *N. pharaonis* SRII; SRII, sensory rhodopsin II; FTIR, Fourier transform infrared spectroscopy; PDB, Protein Data Bank; DDM, *n*-dodecyl-β-D-maltoside.

0022-2836/$ - see front matter

Introduction

Rhodopsin, a membrane protein with retinal as a chromophore, operates as a photoreceptor in animal retinas. In the early 1970s, a retinal-containing membrane protein (retinal protein) was discovered in a halophilic archaeon, *Halobacterium salinarum* (formerly *halobium*). This protein functions as a light-driven proton pump and was named bacteriorhodopsin (BR).[1] Subsequently, three different retinal proteins were found in the same bacterium *H. salinarum*. They are halorhodopsin, sensory rhodopsin I, and sensory rhodopsin II (SRII, also called phoborhodopsin), which are a light-driven anion pump, a photoreceptor for positive and negative phototaxis, and a photoreceptor of negative phototaxis, respectively.[2] After the discovery of the four archaeal rhodopsins, the existence of retinal proteins was considered to be confined to the halophilic Archaea and mammalian retinas. The turning point came with the discoveries of *Neurospora* rhodopsin[3] and proteorhodopsin[4] found in fungi and marine bacteria or plankton, respectively, and subsequently, the existence of retinal proteins has been reported for various organisms, including fungi, algae, eubacteria, and cyanobacteria.[5,6] Rhodopsin (retinal protein) is now considered to be ubiquitous in microorganisms, and this retinal protein is referred to as microbial rhodopsin.[7] The microbial rhodopsins act as ion pumps (usually a proton pump) or sensory receptors. The world of microbial rhodopsins is now expanding.

Two rhodopsins[8] in *Chlamydomonas reinhardtii*, initially identified as photoreceptors in this alga, were found to function as a phototaxis receptor and a light-gated ion channel and were named channel rhodopsin 1 and channel rhodopsin 2. These functions allowed further classification based on the following electrical properties: (1) electrogenic ion pumps, including BR from *H. salinarum*[9] and halorhodopsin from *Natronomonas pharaonis* (NpHR),[10] (2) light-gated channels, such as ChR 1 and ChR 2,[8] and (3) electrically neutral rhodopsins, such as *Anabaena* sensory rhodopsin (ASR)[11] and transducer-bound sensory rhodopsin I and SRII.[2] Note that only the SR's (without transducers) are categorized as light-driven proton pumps.[12] The existence of categories (1) and (2) has fostered the development of a new field, opto-neurophysiology.[13,14] Neuron spiking in nerve cells expressing channel rhodopsins, NpHR, *Acetabularia* rhodopsin (AR), and archaerhodopsin can be controlled by laser light stimuli.[15,16] Furthermore, a modified NpHR was engineered for high expression in neurons and used for ultrafast optogenetics.[17] These applications are feasible because of the following special characteristic of the microbial rhodopsins: repetitive light stimulation can be applied because they have a photocycle. Photoexcitation of microbial rhodopsins leads to the excited state, with the isomerization of retinal from all-*trans* to 13-*cis*, followed by thermal relaxation to the original state *via* various intermediates, the K, L, M, N, and O intermediates.[9,18] In addition, opto-computer or bioelectric devices using BR[19] or SRII[20] have been devised. Thus, studies of microbial rhodopsins are interesting from the viewpoints of biotechnology and neuroscience, as well as their functional mechanisms.

The elucidation of the functional mechanism of microbial rhodopsins (ion transporters or receptors) is eagerly anticipated and would also improve biotechnological devices. Toward this end, many biophysical methods have been applied, and one of the most promising methods is X-ray crystallography. The proton-pumping mechanism of BR has been investigated by spectroscopic methods, such as flash photolysis, Fourier transform infrared spectroscopy (FTIR), and Raman scattering, and the X-ray structures of the ground state and intermediates have contributed greatly to the elucidation of the pumping mechanism.[9] Thus, following the clarification of the BR structure,[21] we have subsequently reported high-resolution crystallographic structures of archaeal[22,23] and eubacterial[24,25] rhodopsins. However, the structure of a eukaryotic rhodopsin has not been solved.

Acetabularia is a giant unicellular and uninucleate marine green alga. As early as 1968, Schilde suggested that rhodopsin could be the photoreceptor of this alga.[26] Tsunoda *et al.* cloned the opsin gene of *Acetabularia acetabulum* and named it AR.[27] In addition, they demonstrated its function as a light-driven proton pump, using oocytes expressing AR. Our screen generated two clones, the full-length AR (with some changes) and another gene similar to AR but with clear differences. The latter was named ARII. The cell-free protein synthesis system supplemented with a steroid-derived detergent and lipid[28] successfully generated a large amount of ARII, which allowed us to perform various experiments. We analyzed the retinal configuration and the photochemistry. We observed the photo-induced outward current through oocyte membranes expressing ARII and the photo-induced proton transfer using a transparent indium tin oxide (ITO) electrode, which works as a time-resolving pH electrode.[29] From these observations, we concluded that ARII is a light-driven ion pump. We successfully obtained ARII crystals that diffracted to a resolution of 3.2 Å, and the structure revealed the characteristic regions likely to be involved in the proton transport. As far as we know, this is the first report on the crystal structure of a eukaryote-derived microbial rhodopsin synthesized functionally by a cell-free synthetic method.

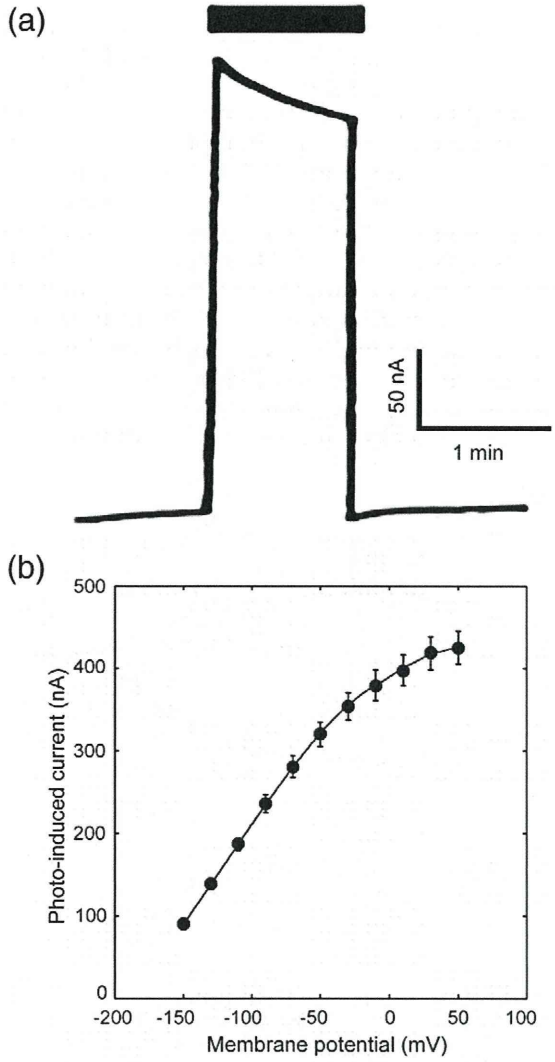

Fig. 1. Photo-induced current in an ARII-expressing *Xenopus* oocyte. (a) A typical trace of the photo-induced current. The top bar indicates the period of illumination with green light. The membrane potential was clamped at −50 mV. (b) Relationship between the photo-induced current and the clamped membrane potential.

Results and Discussion

Identification of AR

The genes encoding the two opsins, ARI and ARII (GenBank accession nos. HM070407 and HM070408), were identified in *Acetabularia* juvenile-specific cDNA by the PCR method. The amino acid sequence of ARI was quite similar to that of AR reported previously,[27] except for the truncation of the C-terminal region. ARII consists of 247 amino acid residues, and its sequence identities with ARI and BR are 56% and 33%, respectively. ARII is similar to, but distinct from, AR (ARI). The amino acid residues in BR that are essential for the proton pumping are all conserved in ARII; these are Asp81 (corresponding to $Asp85^{BR}$), Asp92 ($Asp96^{BR}$), Arg78 ($Arg82^{BR}$), Glu199 ($Glu204^{BR}$), and Asp207 ($Asp212^{BR}$), but $Glu194^{BR}$ is substituted with Ser189. Thus, we expected ARII to be a light-driven proton pump. In experiments where ARII-expressing *Xenopus* oocytes were exposed to a steady green light, a photo-induced outward current was observed (Fig. 1a). The photocurrents increased in a clamp-voltage-dependent manner and reached saturation at the positive voltage (Fig. 1b), with a profile similar to that of ARI (or AR).[27] Therefore, we concluded that ARII is a light-driven ion (probably proton) pump.

Biochemical properties of ARII synthesized using the cell-free system

The expression of the ARII opsin genes in *Escherichia coli* UT5600 with an endogenous retinal biosynthesis system[30] was previously attempted. However, the expression level of the protein was poor (data not shown). Therefore, we utilized the cell-free protein synthesis system, which is unique in that the expression is performed in the presence of both lipid and detergent (for details, see Materials and Methods).[28] We obtained a sufficient amount of ARII to analyze its biochemical features: the yield of ARII from a 27-ml cell-free synthesis reaction was 4.5 mg. The UV–visible absorption spectrum of ARII (Fig. 2) showed a peak at 532 nm due to the opsin shift of retinal,[31,32] indicating that the cell-free-synthesized ARII opsin was folded correctly and bound to the chromophore. The estimated molar extinction coefficient at 530 nm was 40,000, which is approximately equivalent to those of other microbial rhodopsins. An HPLC analysis revealed that the retinal conformations consisted of 94.7% all-*trans* and 5.3% 13-*cis* after exposure to orange light for 5 min and 95.5% all-*trans* and 4.5% 13-*cis* in the dark

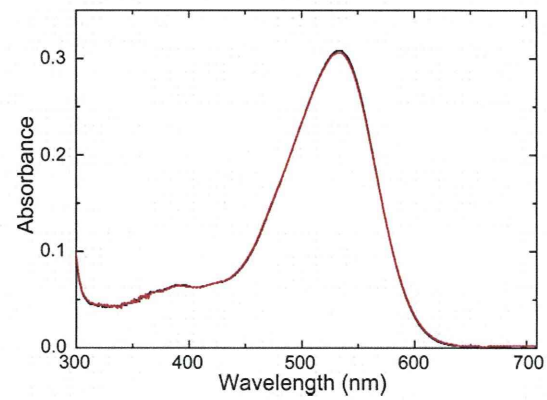

Fig. 2. UV–visible absorption spectra of ARII. The spectra for the samples kept in the dark and exposed to light are shown in black and red, respectively.

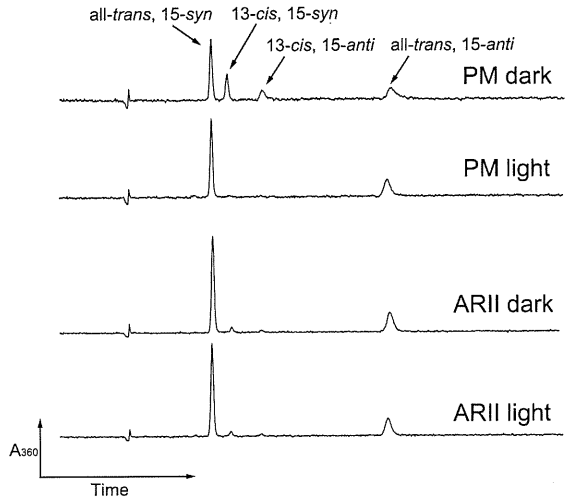

Fig. 3. HPLC analyses for the retinal isomer composition. The terms "dark" and "light" on the chromatograms indicate those obtained using dark- and light-adapted samples, respectively. The upper two chromatograms are those for BR, from which the retention times of the all-*trans*, 15-*syn*; 13-*cis*, 15-*syn*; 13-*cis*, 15-*anti*; and all-*trans*, 15-*anti* isomers of retinal were determined.

(Fig. 3). Unlike BR, no dark adaptation was observed for ARII.

The photochemical reaction of ARII was examined by flash photolysis. Figure 4a shows the time courses of the absorbance change at selected wavelengths for ARII (upper panel), and BR in purple membrane is also shown for comparison (lower panel). Flash-induced depletion and recovery of the original pigment were observed on the trace at 530 nm for ARII and at 570 nm for BR, and the existence of the M and O intermediates was confirmed on the trace at 400 nm and 610 nm for ARII and at 400 nm and 650 nm for BR, respectively. The results shown in Fig. 4a suggest that the photocycle scheme of ARII is similar to that of BR. Similar to BR,[9,33] the photocycling rate of ARII was on the millisecond timescale, resembling that of a typical light-driven proton pump. The M formation by ARII occurs earlier than that of BR. Experiments with a faster time resolution are necessary to examine this in detail. According to our preliminary results (experiments are now in progress), the decay of the K intermediate of ARII almost immediately led to the formation of M (also see Fig. 4a), and then the L intermediate of ARII was difficult to observe. Thus, the appearance of M in ARII may be earlier than that in BR. The significance of the different behaviors among the earlier photochemical intermediates is not clear at present. The fast photocycle

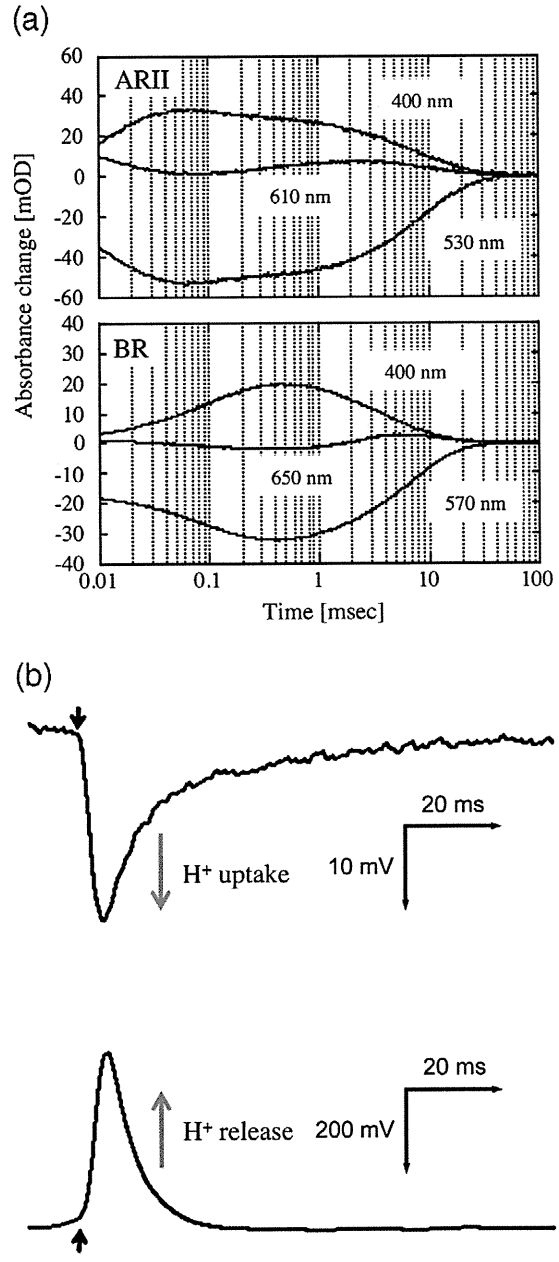

Fig. 4. Flash-induced absorbance changes at selected wavelengths (a) and voltage change of the ITO electrode (b) for ARII (upper panel) and BR (lower panel). (a) Flash-induced absorbance changes at 530 and 570 nm to monitor the depletion/recovery of the original pigments of ARII and BR, respectively. Those at 400 nm represent the formation/decay of M intermediates, and those at 610 and 650 nm represent the formation/decay of O intermediates of ARII and BR, respectively. ARII, solubilized with 0.05% DDM, was suspended in 400 mM NaCl at pH 7 adjusted with 10 mM 6-mix buffer (citrate/4-morpholineethanesulfonic acid/Mops/Hepes/*N*-cyclohexyl-3-aminopropanesulfonic acid/Ches). BR was measured in 50 mM Tris–HCl, pH 7.0, with 400 mM NaCl. The temperature was 20 °C. (b) Proton transfers by ARII reconstituted into egg PC (upper panel) and BR in purple membrane (lower panel) were measured with an ITO transparent electrode. The medium was 400 mM NaCl buffered with 1 mM 6-mix buffer (pH 7.0). The arrow shows the excitation time with a 2-ms light pulse.

is consistent with ARII functioning as a light-driven ion pump, as shown in Fig. 1. To identify the transported ion species, we performed measurements with an ITO transparent electrode, which works as a time-resolving pH electrode,[29,34] and observed the voltage changes after excitation by a Xenon light pulse (Fig. 4b). Since a downward shift of the ITO signals indicates a decreasing proton concentration, we concluded that the proton uptake by ARII precedes the release at pH 7.0, in contrast to that by BR. Combined with the observations shown in Fig. 1, during the ARII photocycle, proton uptake from the cytoplasm occurs first, followed by release to the extracellular side. By contrast, it is well known that flash illumination of BR first induces proton release, followed by proton uptake at pH 7.0 (Fig. 4b).[35] These observations revealed that ARII acts as a light-driven proton pump. The possible origin of the reversed sequence of the proton release/uptake will be described later.

During a photocycle, BR releases a proton with the formation of the M intermediate and uptakes a proton with the decay of the N intermediate.[35] In the case of ARII, this sequence of proton release and uptake is reversed relative to that in BR. Simultaneous measurements of the rise/decay of photointermediates and pH changes in the medium using pyranin showed that the proton uptake occurred with the formation of the O intermediate, and the release occurred with the decay of the O intermediate (T. Kikukawa *et al.*, unpublished results). Later proton release has also been observed in the fungal rhodopsins from *Neurospora*[36] and *Leptosphaeria*,[37] proteorhodopsin,[38] archaerhodopsin 4,[39] and mutants of BR that lack the proton release group.[40,41] The later proton release by these rhodopsins may be a consequence of the inefficiency of the residue regulating proton release. The difference in the proton transfer sequences between BR and ARII may be caused by the lack of a residue that functions as a proton-releasing group [Ser189 ($Glu194^{BR}$)] and/or the different pK_a of the residue [Glu199 ($Glu204^{BR}$)] from which the proton is released to the extracellular space. Note that, in spite of the low resolution, the absence of water molecules near the proton-releasing group is suggested in the crystal structure described below, in contrast to the wild-type BR.

Crystal structure of ARII

ARII, synthesized by the cell-free protein synthesis system with detergent/lipid, was crystallized by the *in meso* method using monoolein,[42] and many reddish-purple plate-like crystals grew to sizes of 100 μm × 100 μm × 10 μm at 20 °C within 2 weeks. One of the advantages of the cell-free membrane protein synthesis system with detergent/lipid is that the content of the synthesized target protein in the liposome is high enough to enable a one-step purification procedure. In addition, using this cell-free synthesis and mesophase crystallization method, we retain the membrane proteins in the lipid environment, which is advantageous for unstable proteins during solubilization and purification. The purity and the absorption of the ARII protein used for crystallization are shown in Fig. 5. The absorption ratio was 1.34 (280 nm/532 nm). The crystal structure of ARII, consisting of seven helices (A to G) and a retinal molecule (Fig. 6a), was determined at 3.2 Å resolution (Table 1). Four ARII proteins with eight cholesterol molecules were observed in the asymmetric unit (Fig. 6b). The cholesterol molecules were located between helices A and G of one ARII molecule and helix A of the ARII molecule from the neighboring asymmetric unit. These intermolecular contacts

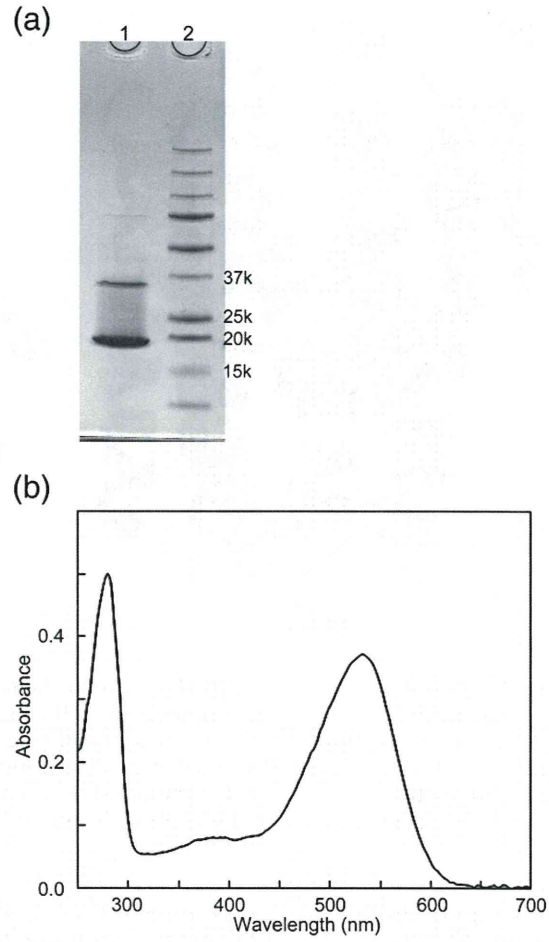

Fig. 5. Purified ARII protein used for crystallization. (a) The 10–20% gradient SDS-PAGE image for the purified ARII protein (lane 1), with molecular mass markers (lane 2). The two bands around 18 and 35 kDa in lane 1 represent the monomer and the dimer of ARII, respectively. (b) The absorption spectrum shows a peak at 280 nm.

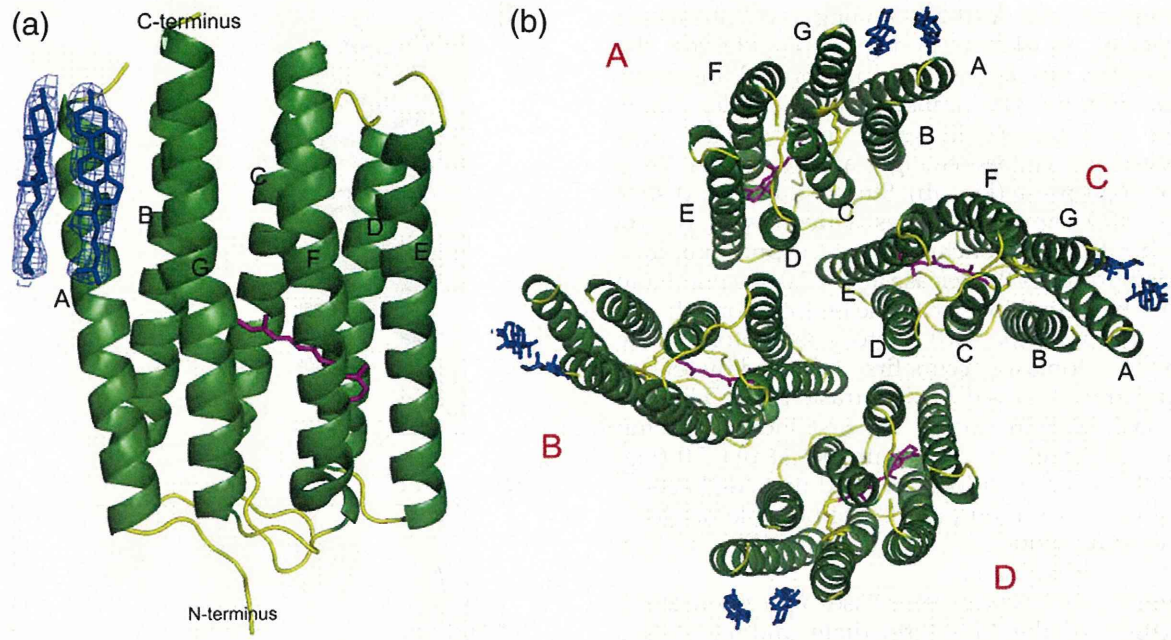

Fig. 6. Crystal structures of ARII. The seven α-helices (A to G) and the loops in the opsin are shown in green and yellow, respectively. The organic compounds, retinal and cholesterol, are shown in magenta and blue, respectively. (a) ARII monomer structure. The C- and N-terminal sides of ARII correspond to the cytoplasmic and extracellular sides, respectively. The $F_o - F_c$ omit electron density maps around cholesterol are shown, with a contour level of 1.0 σ. (b) A view of the asymmetric unit from the C-terminal side. There is a non-crystallographic symmetry axis around the four ARII monomers (A to D; shown in red letters) with eight cholesterols.

should play important roles in stabilizing the overlaid planar layers of ARII in the thin plate-like crystal. No obvious electron densities for the loops between helices A and B and between helices E and F were found in the map. These regions contact another crystal layer on the C-terminal side of ARII. A structural alignment (Fig. 7) performed by the Dali server[43] revealed that the ARII structure is quite similar to those of other rhodopsins, such as BR [Protein Data Bank (PDB) ID 1C3W, Z score=28.9],[21] *N. pharaonis* SRII (NpSRII; also called *pharaonis* phoborhodopsin) (PDB ID 1H68, Z score=29.3),[22] and ASR (PDB ID 1XIO, Z score=27.8).[24] The highly conserved regions of helix C and the C-terminal portion of helix F might participate in a common mechanism for ion pumping and photo sensing by rhodopsin because the local flex of helix C at the L intermediate and the outward movement of helix F at the M2 intermediate have been observed in BR[44,45] and NpSRII.[46,47]

In helix G, the carbonyl groups of Val208 and Leu209 form hydrogen bonds with the amide NH groups of Leu213 and Asn214, respectively. These interactions create a π-bulge and kink the helix at Lys211, which is bound with the all-*trans* retinal chromophore and forms a Schiff base (Fig. 8). The side chains of Phe134, Cys138, Gln141, Trp178, Tyr181, and Trp185 are located within 3.5 Å of the polyene chain of the retinal. The BR structure at 1.55 Å resolution revealed that the Wat501 water molecule interacts with the carbonyl group of Ala215 and the indole ring of Trp182 and helps to stabilize the retinal.[21] Although no electron density was observed between the carbonyl group of Ala210 and the indole nitrogen atom of Trp178 at a 5.6-Å distance in the map, a water molecule may interact with these residues.

The retinal binding site in ARII is very similar to that in BR. However, we observed only a small amount of the 13-*cis* conformation of retinal in ARII in the dark, unlike BR (also see the HPLC results in Fig. 3). NpSRII also has only all-*trans* retinal, and the relative positions of the protonated Schiff base and the counterion are important for light–dark adaptation.[48,49] Furthermore, based on analyses using the chimeric protein between BR and NpSRII, we previously reported that the alteration around the β-ionone ring, by the interaction between helices D and E, might cause the counterion region to change through the polyene chain of the retinal.[50] A comparison of the BR, NpSRII, and ARII structures revealed differences in some hydrogen bonds around the β-ionone ring in helix E.[21,22] In BR, which has all-*trans* and 13-*cis* retinal in the dark, the ε1 nitrogen atom of Trp138, the γ1 oxygen atom of Ser141, and the γ1 oxygen atom of Thr142 interact with the oxygen atom of the main chain of Pro186

Table 1. X-ray data collection and refinement statistics

Data collection	
Wavelength (Å)	1.0000
Resolution range (Å)	50.00–3.20
Space group	$P2_12_12_1$
Unit cell parameters	
$a/b/c$ (unit cell, Å)	84.1/110.5/129.1
Reflections	
Measured	89,274
Unique	18,284
Completeness (%)	
Overall	89.5
Outer shell	(3.31–3.20 Å) 72.2
R_{sym} (%)[a]	
Overall	11.5
Outer shell	(3.31–3.20 Å) 25.1
Redundancy (overall)	4.9
Mean $\langle I/\sigma(I)\rangle$	
Overall	11.3
Outer shell	(3.31–3.20 Å) 3.3
σ cutoff	0.0
Refinement	
R_{cryst}/R_{free} (%)[b]	29.0/32.4
r.m.s.d. bond lengths (Å)	0.011
r.m.s.d. bond angles (°)	1.4
Average *B*-factor (Å^2)	24.1
Number of retinal molecules	4
Number of cholesterol molecules	8
Ramachandran plot (%)	
Residues in most favorable regions	88.6
Residues in additional allowed regions	11.4
Residues in generously allowed regions	0.0

[a] $R_{sym} = \sum |I_i - \langle I\rangle| / \sum |I_i|$, where I_i is the intensity of an observation and $\langle I\rangle$ is the mean value for that reflection, with the summations over all reflections.

[b] $R_{cryst} = \sum h ||F_o(h)| - |F_c(h)|| / \sum h F_o(h)$, where F_o and F_c are the observed and calculated structure factor amplitudes, respectively. R_{free} was calculated with 4.9% of the data excluded from the refinement.

(F helix), Met118 (D helix), and Trp138, respectively. These residues are Phe134, Gly137, and Cys138 in ARII and Phe127, Gly130, and Ala131 in NpSRII, respectively, and no hydrogen bonds are formed. The importance of the methionine residue (Met145 of BR[51] and BR homologues[52]) was reported: the BR mutant M145A increased the all-*trans* content, suggesting that the existence of the bulky methionine increases the 13-*cis* content. On the other hand, for NpSRII with only all-*trans* retinal, the F134M mutation increased the 13-*cis* content.[48,50] This might be a consequence of the relatively wide retinal binding pocket of NpSRII. Similarly, the pocket in ARII is wide, which might mitigate the effect of the replacement of Gln141 with Met (the Q141M mutant). However, ARII is a good system to test this hypothesis, and examinations of the retinal configurations of the mutant proteins with the above-described residues (especially Q141M), as well as analyses of the crystal structures, should be performed in the future.

Proton transfer mechanism

At the transition from the L state to the M state in the BR photocycle, a proton is transferred from the protonated Schiff base to the carboxyl oxygen atoms of Asp85. The Schiff base is hydrogen bonded to a water molecule, which forms a hydrogen-bond network with Asp85, Asp212, Arg82, and two water molecules.[21,53] A proton is then released to the extracellular space from the proton release group, consisting of Arg82, Glu194, and Glu204. Recently, it was suggested that Glu194 and Glu204

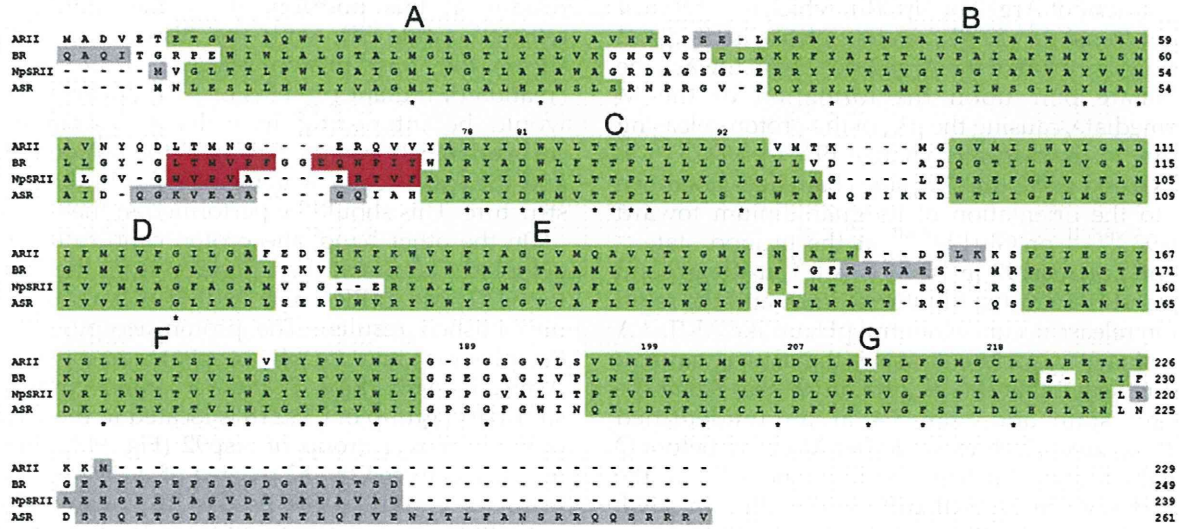

Fig. 7. Structure-based sequence alignment of ARII with BR and ASR. The α-helices, β-strands, and undetermined regions are shown in green, red, and gray, respectively. The identical residues in the sequence alignment are marked by asterisks. The residue numbers are provided in the column on the right side of the alignments and above the ARII residues involved in the proton transfer.

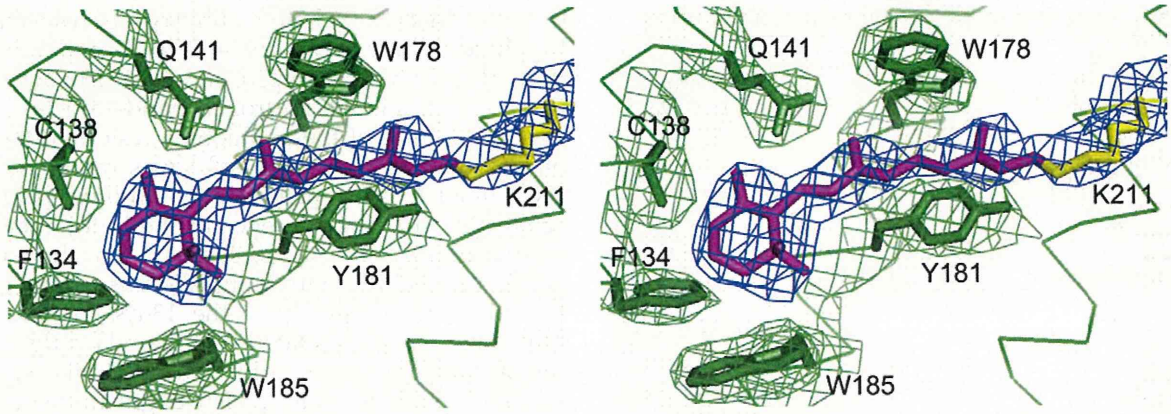

Fig. 8. Stereo diagram of the retinal chromophore bound to the side chain of Lys211, surrounded by Phe134, Cys138, Gln141, Trp178, Tyr181, and Trp185. The stick models of retinal, Lys211, and the surrounding six residues are colored magenta, yellow, and green, respectively. The $2F_o - F_c$ electron density map for these models is contoured at 1.0 σ. The C^α backbones are represented by lines.

in BR are bonded by a delocalized proton, and a low-barrier hydrogen bond might be advantageous for rapid proton release.[54]

In ARII, rapid proton release does not occur at neutral pH. We compared the structure of the proton release pathway in ARII with those in BR and NpSRII. The structure-based alignment diagram (Fig. 7) indicates that Asp85, Asp212, Arg82, Glu194, and Glu204 in BR correspond to Asp81, Asp207, Arg78, Ser189, and Glu199 in ARII and Asp75, Asp201, Arg72, Pro183, and Asp193 in NpSRII. The superposition of the crystal structure of ARII onto that of BR shows that the side chains of these residues fit well with those of BR (Fig. 9a). However, the orientation of the Arg78 side chain is opposite to the corresponding Arg82 of BR but the same as that of Arg72 of NpSRII, which is capable of proton transfer.[12] In BR, proton release is triggered by the movement of the Arg82 side chain toward the glutamate pair upon the formation of the M intermediate, causing the pK_a of the proton-releasing residue to dramatically change (9.7 to 5.7).[55–57] In NpSRII and ARII, this Arg side chain does not move due to the orientation of its guanidinium toward $Asp193^{NpSRII}$ or $Glu199^{ARII}$ at the ground state.[22] The pK_a of Asp193 in NpSRII is 6.4 at the ground state and is 4.9 at the M intermediate, and the rapid proton release occurs at neutral pH, unlike ARII.[34] A preliminary experiment using the E199Q mutant ARII revealed that the pK_a of Glu199 was 9.3 at the ground state and was 8.4 at an unidentified intermediate, which existed after M decay before O formation (unpublished results). The pK_a at the ground state in NpSRII differs from that in ARII, although the orientations of the Arg side chains are similar to each other. These differences might affect the environment around Asp193 or Glu199 and, thus, might be related to the timing of the proton release. Glu199 in ARII may exist in a more hydrophobic region, as compared with Asp193 in NpSRII, and a water molecule (Wat405) interacts with the δ1 oxygen atom of Asp193 and the η1 nitrogen atom of Arg72.[22] No electron density between the ε1 oxygen atom of Glu199 and the η1 nitrogen atom of Arg78 at a 3.5-Å distance in the map was observed. Therefore, a water molecule may not exist around Glu199 and Arg78 in ARII. This may disrupt the formation of the low-barrier hydrogen bond at Glu199, resulting in the "late proton release". Further experiments using FTIR are required to confirm this hypothesis.

The other important residue that may affect the timing of the proton release is $Ser189^{ARII}$, which corresponds to $Glu194^{BR}$ and $Pro183^{NpSRII}$. Note that ARII and NpSRII, containing the non-dissociable residue at this position, show the "late proton release", while BR, with the dissociable residue, shows the "fast proton release". Therefore, the creation of mutant proteins of ARII at this position would be interesting in order to examine the correlation between the timing of the proton release and the existence of water molecules in the crystal structure. This should be performed in the future.

On the other hand, the proton capture from the cytoplasm occurs at the transition from the N state to the O state in BR[35] and ARII (T. Kikukawa *et al.*, unpublished results). The proton acceptor on the cytoplasmic side in BR (Asp96) corresponds to Asp92 in ARII (Figs. 7 and 9a). Interestingly, the sulfhydryl group of Cys218 is located in the vicinity of the carboxyl group of Asp92 (Fig. 9b), and the distance between the δ2 oxygen of Asp92 and the γ sulfur of Cys218 is 3.9 Å. Cys218 corresponds to Leu223 in BR (Fig. 9c) and to Asp217 in ASR (Fig. 9d) and is unique to ARII. The FTIR spectrum for ASR showed a broad positive band at 1740–1700 cm^{-1}, indicating the protonation of $Asp217^{ASR}$ in the M intermediate.[58] The D217E mutant of ASR

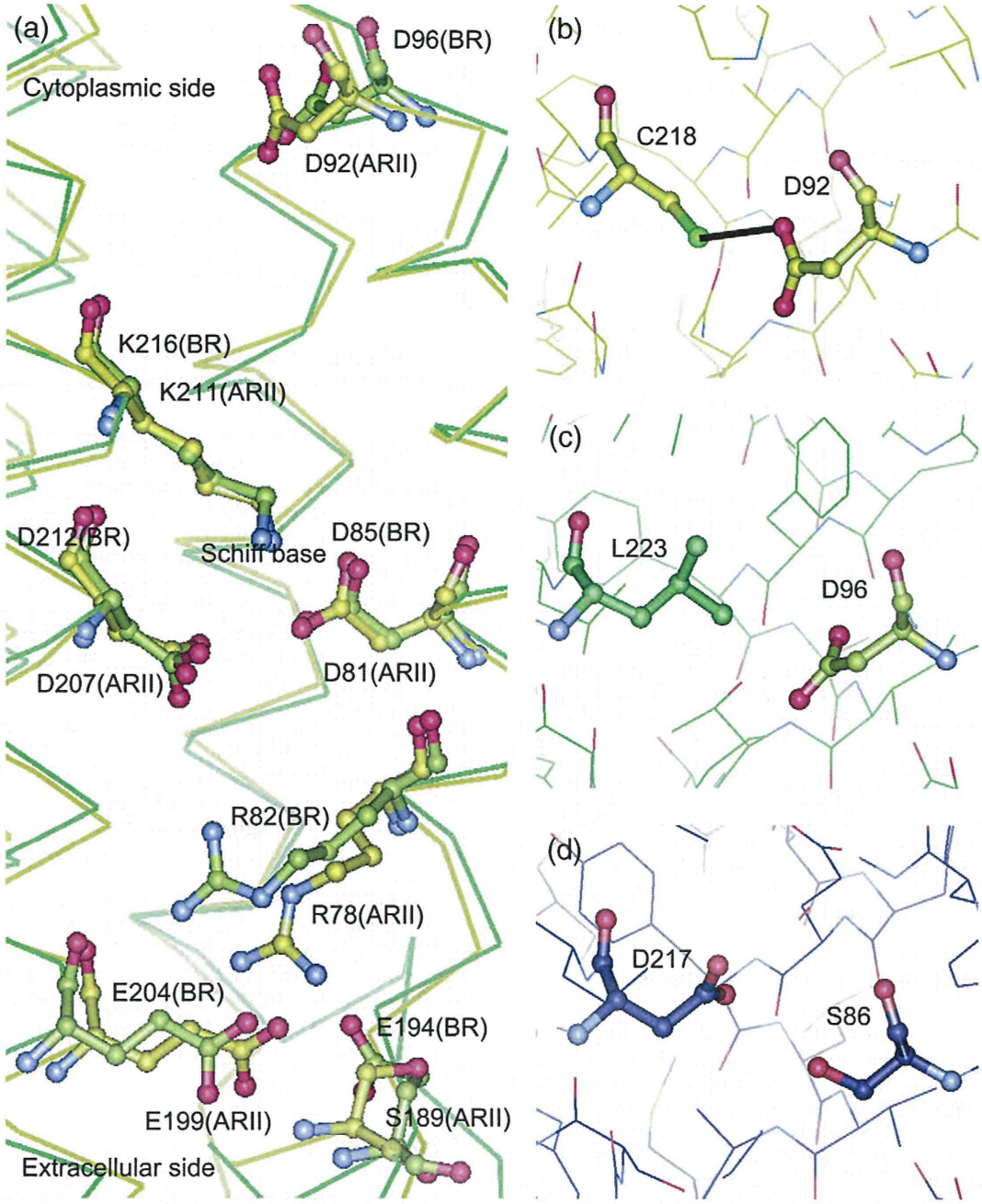

Fig. 9. Amino acid residues involved in the proton transfer. (a) Superimposition of the ARII and BR structures colored yellow and green, respectively. The amino acid residues directly involved in the proton transfer in BR and the corresponding residues in ARII are shown with ball-and-stick models, while the C^{α} backbones of the ARII and BR helices are shown with wire models. The Asp92, Lys211 (Schiff base), Asp207, Asp81, Arg78, Glu199, and Ser189 residues of ARII correspond to the Asp96, Lys216 (Schiff base), Asp212, Asp85, Arg82, Glu204, and Glu194 residues of BR. A proton is transferred from the cytoplasmic side to the extracellular side through the proteins. (b) Asp92 and Cys218 of ARII. The distance between the δ2 oxygen atom of Asp92 and the sulfur atom of Cys218 is 3.0 Å, as indicated with a black line. Cys218 is likely to be involved in proton uptake from the cytoplasm. (c) Asp96 and Leu223 of BR correspond to Asp92 and Cys218 of ARII, respectively. (d) Ser86 and Asp217 of ASR correspond to Asp92 and Cys218 of ARII, respectively.

displayed inward proton transport activity,[59] and Kawanabe *et al.* concluded that this transport activity is correlated with the proton affinity at position 217 of ASR.[60] Therefore, the side chain of Cys218 in ARII may play an important role in proton uptake. A low-barrier hydrogen bond might exist between Asp92 and Cys218 in order to promote proton uptake in ARII. Preliminary results

on the Cys218 mutant of ARII are indicative of an interaction with the proton–donor residue Asp92, and detailed experiments are now underway.

Materials and Methods

Measurements of photo-induced current across oocyte membranes expressing ARII

The genes encoding the two opsins, ARI and ARII, were cloned from an *Acetabularia* juvenile-specific cDNA library by PCR, using both directional primers for the conserved amino acid sequence RYIDW. *Acetabularia* uses TAA and TAG as glutamine codons and TGA as the only stop codon; thus, we changed these sequences.[61] The ARII gene, truncated at position 229, was inserted into the plasmid pGH19 to synthesize the capped complementary RNA encoding ARII, using a mMESSAGE mMACHINE kit (Ambion Inc., Austin, TX).[62] Mature oocytes at stages V and VI from *Xenopus* were isolated by a treatment with 1.6 mg/ml of collagenase manually defolliculated and maintained at 18 °C in a modified Barth's medium supplemented with 3 mM retinal and 50 mg/ml gentamicin. On the following day, the oocytes were injected with 50 ng complementary RNA encoding the ARII gene and incubated for 3–5 days. Electrophysiological studies were performed by the two-electrode voltage clamp technique, as described previously.[62] The oocyte was voltage clamped at −50 mV and superfused with the standard buffer [10 mM Hepes/Tris (pH 7.5), 100 mM NaCl, 2 mM KCl, 1 mM $MgCl_2$, and 1 mM $CaCl_2$]. The photo-induced currents were measured during steady illumination with 530+18 nm of green light from a light-emitting diode (Luxeon V Star) (LXHL-LM5C; Philips Lumileds Lighting Company, San Jose, CA).

Preparation of ARII by cell-free synthesis

The ARII gene from the plasmid for expression in *Xenopus* oocytes was cloned into the plasmid pCR2.1-TOPO for cell-free synthesis supplemented with 0.4% (w/v) digitonin (Wako, Osaka, Japan) and 6.7 mg/ml phosphatidylcholine (Sigma, St. Louis, MO). The procedures for the cell-free synthesis and purification of ARII were the same as those employed for BR,[28] except that 20 mM Tris–HCl (pH 7.0) buffer containing 400 mM NaCl, 1 mM dithiothreitol, 10% glycerol, and 0.01% *n*-dodecyl-β-D-maltoside (DDM; Anatrace, Maumee, OH) was used for the gel-filtration chromatography. The final fractions were concentrated to 45.4 mg/ml with a filter unit for crystallization. For the biochemical assay, ARII was purified by Ni^{2+} chelating affinity chromatography, and the modified histidine tag (N11-tag)[63] at the N-terminus was not removed. The concentration was determined by the absorption at 280 nm using the extinction coefficient.[64]

Spectroscopic analyses

The ARII solution was kept in the dark for 5 days at room temperature, and then the absorption spectrum of the dark-adapted sample was measured in the range between 300 and 700 nm using a UV-1800 spectrophotometer (Shimadzu, Kyoto, Japan). The ARII solution was exposed to green light at 530 nm from a high-power light-emitting diode (LXHL-LM5C; Philips Lumileds Lighting Company) for 5 min to prepare the light-adapted sample, followed by the spectroscopic measurements in the same manner. After methanol and hydroxylamine were added to each of the dark- and light-adapted ARII solutions, the retinal oximes were extracted with hexane and subjected to an HPLC analysis (LC-10AT) and UV–visible detection (Shimadzu). The HPLC analyses for the retinal isomer composition were performed as described previously.[48]

Measurements of photo-induced proton transfer with the ITO transparent electrode and flash photolysis

Purified N11-tag-fused ARII proteins were reconstituted into phosphatidylcholine at an ARII:phosphatidylcholine molar ratio of 1:100 and suspended in distilled water.[34] The suspensions (100 μl) of 10–30 μM ARII or purple membranes from *H. salinarum* in 1 mM 6-mix buffer [citrate, 4-morpholineethanesulfonic acid, Mops, Hepes, *N*-cyclohexyl-3-aminopropanesulfonic acid, and Ches (pH 7.0)] and 400 mM NaCl were applied to the surface of an ITO transparent electrode (Techno Print Co., Ltd., Saitama, Japan). After an incubation in an evaporator for ~60 min to dry the sample, the electrode was thoroughly washed with distilled water to remove the unbound proteins. The sample was excited with a 2-ms light pulse using a mechanical shutter. The light was generated by a 300-W Xenon lamp through a cold mirror, an infrared cut filter, and cutoff optical filters (Toshiba, Tokyo, Japan). The signals from the ITO electrode were fed to a 0.08-Hz low-cut filter to remove the baseline fluctuation.[34]

The absorption changes of ARII were monitored after photoexcitation with a Nd-YAG laser pulse (532 nm, 7 ns) using the apparatus described previously.[65] The temperature was maintained at 20 °C. The buffers were 400 mM NaCl containing 0.05% DDM for ARII (with the pH adjusted to 7.0 with 10 mM 6-mix buffer) and 50 mM Tris–HCl (pH 7.0) containing 400 mM NaCl for purple membrane.

Crystallography

ARII was crystallized by the *in meso* method using monoolein as the host lipid.[42,66] The purified protein solution, monoolein, and cholesterol (40:54:6 w/w) were homogenized with a micro syringe-based mixing device with a monolithic stainless steel coupler,[67,68] and a 100-nl portion of the homogenized mixture was placed on a glass plate well (6 mm in diameter, 135 μm in thickness) using a laboratory-constructed micro-dispenser. The mixture was then sealed with a glass coverslip after 1.0 μl of a precipitant solution containing 0.1 M Tris–HCl (pH 7.5), 6% 2-methyl-2,4-pentanediol, and 14% polyethylene glycol 400 was overlaid on the mixture. The glass plates for crystallization were incubated at 20 °C for 2 weeks. A 100 μm×100 μm×10 μm size crystal was picked with a MicroSieve tool (MiTeGen, Ithaca, NY) from the lipidic mesophase and flash cooled in a nitrogen stream at −180 °C, as soon as the seal of the glass plate was opened,

in the BL41XU beamline at SPring-8. The ARII crystals were very unstable under the open-air conditions and were easily damaged during handling with the micro tool. Thus, the crystal picking and diffraction check were performed repeatedly until diffraction pattern images that could be indexed were obtained. Data collection was performed using a 10-μm-size microbeam with a Mar MX-225HE detector. The data set was integrated and scaled to 3.2 Å resolution using the program HKL2000.[69] Initial phases were determined by molecular replacement using the model (PDB ID 1S54) of BR from *H. salinarum* with the program MrBUMP in the CCP4 program suite.[70] The coordinates were refined with the program CNS version 1.2[71] and were manually rebuilt with non-crystallographic symmetry using the program Coot.[72]

Accession number

The crystallographic coordinates of ARII have been deposited in the PDB with the accession code 3AM6.

Acknowledgements

We thank Prof. Dina F. Mandoli at The University of Washington for providing information about the partially cloned ARI and ARII genes, Dr. Yoshiaki Kawano and Dr. Masaki Yamamoto for their assistance at BL41XU in SPring-8, and Prof. Tsutomu Kouyama at Nagoya University for providing the input files for the CNS program. This work was supported by the Targeted Proteins Research Program. Additional support was provided by the National Research Foundation of Korea (NRF 331-2008-1-C00242) and the 21C Frontier Microbial Genomics and Application Center Program, Ministry of Education, Science and Technology, Korea, to K.H.J. and the second stage of the Brain Korea 21 graduate Fellowship Program to S.Y.K.

References

1. Oesterhelt, D. & Stoeckenius, W. (1973). Functions of a new photoreceptor membrane. *Proc. Natl Acad. Sci. USA*, **70**, 2853–2857.
2. Spudich, J. L. & Jung, K.-H. (2005). Microbial Rhodopsins: Phylogenetic and Functional Diversity. In *Handbook of Photosensory Receptors* (Briggs, W. R. & Spudich, J. L., eds), pp. 1–23, Wiley-VCH Verlag GmbH & Co. KGaA, Weinheim, Germany.
3. Bieszke, J. A., Spudich, E. N., Scott, K. L., Borkovich, K. A. & Spudich, J. L. (1999). A eukaryotic protein, NOP-1, binds retinal to form an archaeal rhodopsin-like photochemically reactive pigment. *Biochemistry*, **38**, 14138–14145.
4. Béjà, O., Aravind, L., Koonin, E. V., Suzuki, M. T., Hadd, A., Nguyen, L. P. *et al.* (2000). Bacterial rhodopsin: evidence for a new type of phototrophy in the sea. *Science*, **289**, 1902–1906.
5. Adrian, L., Ouyang, Z., Tseng, Y.-Y. & Liang, J. (2006). Evolutionary pattern of retinal-binding pockets of type I rhodopsin and their functions. *Photochem. Photobiol.* **82**, 1426–1435.
6. Jung, K.-H. (2007). The distinct signaling mechanism of microbial sensory rhodopsins in Archaea, Eubacteria and Eukarya. *Photochem. Photobiol.* **83**, 63–69.
7. Spudich, J. L., Yang, C.-S., Jung, K.-H. & Spudich, E. N. (2000). Retinylidene proteins: structures and functions from archaea to humans. *Annu. Rev. Cell Dev. Biol.* **16**, 365–392.
8. Nagel, G., Szellas, T., Kateriya, S., Adeishvili, N., Hegemann, P. & Bamberg, E. (2005). Channelrhodopsins: directly light-gated cation channels. *Biochem. Soc. Trans.* **33**, 863–866.
9. Lanyi, J. K. (2006). Proton transfers in the bacteriorhodopsin photocycle. *Biochim. Biophys. Acta*, **1757**, 1012–1018.
10. Duschl, A., Lanyi, J. K. & Zimányi, L. (1990). Properties and photochemistry of a halorhodopsin from the haloalkalophile, *Natronobacterium pharaonis*. *J. Biol. Chem.* **265**, 1261–1267.
11. Jung, K.-H., Trivedi, V. D. & Spudich, J. L. (2003). Demonstration of a sensory rhodopsin in eubacteria. *Mol. Microbiol.* **47**, 1513–1522.
12. Sudo, Y., Iwamoto, M., Shimono, K., Sumi, M. & Kamo, N. (2001). Photo-induced proton transport of *pharaonis* phoborhodopsin (sensory rhodopsin II) is ceased by association with the transducer. *Biophys. J.* **80**, 916–922.
13. Bamann, C., Nagel, G. & Bamberg, E. (2010). Microbial rhodopsins in the spotlight. *Curr. Opin. Neurobiol.* **20**, 610–616.
14. Zhang, F., Gradinaru, V., Adamantidis, A. R., Durand, R., Airan, R. D., de Lecea, L. & Deisseroth, K. (2010). Optogenetic interrogation of neural circuits: technology for probing mammalian brain structures. *Nat. Protoc.* **5**, 439–456.
15. Zhang, F., Wang, L.-P., Brauner, M., Liewald, J. F., Kay, K., Watzke, N. *et al.* (2007). Multimodal fast optical interrogation of neural circuitry. *Nature*, **446**, 633–639.
16. Chow, B. Y., Han, X., Dobry, A. S., Qian, X., Chuong, A. S., Li, M. *et al.* (2010). High-performance genetically targetable optical neural silencing by light-driven proton pumps. *Nature*, **463**, 98–102.
17. Gradinaru, V., Zhang, F., Ramakrishnan, C., Mattis, J., Prakash, R., Diester, I. *et al.* (2010). Molecular and cellular approaches for diversifying and extending optogenetics. *Cell*, **141**, 154–165.
18. Hirai, T., Subramaniam, S. & Lanyi, J. K. (2009). Structural snapshots of conformational changes in a seven-helix membrane protein: lessons from bacteriorhodopsin. *Curr. Opin. Struct. Biol.* **19**, 433–439.
19. Wise, K. J., Gillespie, N. B., Stuart, J. A., Krebs, M. P. & Birge, R. R. (2002). Optimization of bacteriorhodopsin for bioelectronic devices. *Trends Biotechnol.* **20**, 387–394.
20. Roy, S., Kikukawa, T., Sharma, P. & Kamo, N. (2006). All-optical switching in *pharaonis* phoborhodopsin protein molecules. *IEEE Trans. Nanobioscience*, **5**, 178–187.

21. Luecke, H., Schobert, B., Richter, H. T., Cartailler, J. P. & Lanyi, J. K. (1999). Structure of bacteriorhodopsin at 1.55 Å resolution. *J. Mol. Biol.* **291**, 899–911.
22. Royant, A., Nollert, P., Edman, K., Neutze, R., Landau, E. M., Pebay-Peyroula, E. & Navarro, J. (2001). X-ray structure of sensory rhodopsin II at 2.1-Å resolution. *Proc. Natl Acad. Sci. USA*, **98**, 10131–10136.
23. Kouyama, T., Kanada, S., Takeguchi, Y., Narusawa, A., Murakami, M. & Ihara, K. (2010). Crystal structure of the light-driven chloride pump halorhodopsin from *Natronomonas pharaonis*. *J. Mol. Biol.* **396**, 564–579.
24. Vogeley, L., Sineshchekov, O. A., Trivedi, V. D., Sasaki, J., Spudich, J. L. & Luecke, H. (2004). *Anabaena* sensory rhodopsin: a photochromic color sensor at 2.0 Å. *Science*, **306**, 1390–1393.
25. Luecke, H., Schobert, B., Stagno, J., Imasheva, E. S., Wang, J. M., Balashov, S. P. & Lanyi, J. K. (2008). Crystallographic structure of xanthorhodopsin, the light-driven proton pump with a dual chromophore. *Proc. Natl Acad. Sci. USA*, **105**, 16561–16565.
26. Schilde, C. (1968). Rapid photoelectric effect in the algae *Acetabularia*. *Z. Naturforsch. T.b*, **23**, 1369–1376.
27. Tsunoda, S. P., Ewers, D., Gazzarrini, S., Moroni, A., Gradmann, D. & Hegemann, P. (2006). H^+-pumping rhodopsin from the marine alga *Acetabularia*. *Biophys. J.* **91**, 1471–1479.
28. Shimono, K., Goto, M., Kikukawa, T., Miyauchi, S., Shirouzu, M., Kamo, N. & Yokoyama, S. (2009). Production of functional bacteriorhodopsin by an *Escherichia coli* cell-free protein synthesis system supplemented with steroid detergent and lipid. *Protein Sci.* **18**, 2160–2171.
29. Tamogami, J., Kikukawa, T., Miyauchi, S., Muneyuki, E. & Kamo, N. (2009). A tin oxide transparent electrode provides the means for rapid time-resolved pH measurements: application to photoinduced proton transfer of bacteriorhodopsin and proteorhodopsin. *Photochem. Photobiol.* **85**, 578–589.
30. Wang, W.-W., Sineshchekov, O. A., Spudich, E. N. & Spudich, J. L. (2003). Spectroscopic and photochemical characterization of a deep ocean proteorhodopsin. *J. Biol. Chem.* **278**, 33985–33991.
31. Shimono, K. & Kamo, N. (2004). Amino acid residues regulating the color among archaeal rhodopsins. *Recent Res. Dev. Photochem. Photobiol.* **7**, 19–38.
32. Nielsen, M. B. (2009). Model systems for understanding absorption tuning by opsin proteins. *Chem. Soc. Rev.* **38**, 913–924.
33. Spudich, J. L. (2006). The multitalented microbial sensory rhodopsins. *Trends Microbiol.* **376**, 480–487.
34. Iwamoto, M., Hasegawa, C., Sudo, Y., Shimono, K., Araiso, T. & Kamo, N. (2004). Proton release and uptake of *pharaonis* phoborhodopsin (sensory rhodopsin II) reconstituted into phospholipids. *Biochemistry*, **43**, 3195–3203.
35. Balashov, S. P. (2000). Protonation reactions and their coupling in bacteriorhodopsin. *Biochim. Biophys. Acta*, **1460**, 75–94.
36. Brown, L. S., Dioumaev, A. K., Lanyi, J. K., Spudich, E. N. & Spudich, J. L. (2001). Photochemical reaction cycle and proton transfers in *Neurospora* rhodopsin. *J. Biol. Chem.* **276**, 32495–32505.
37. Waschuk, S. A., Bezerra, A. G., Jr, Shi, L. & Brown, L. S. (2005). *Leptosphaeria* rhodopsin: bacteriorhodopsin-like proton pump from a eukaryote. *Proc. Natl Acad. Sci. USA*, **102**, 6879–6883.
38. Dioumaev, A. K., Brown, L. S., Shih, J., Spudich, E. N., Spudich, J. L. & Lanyi, J. K. (2002). Proton transfers in the photochemical reaction cycle of proteorhodopsin. *Biochemistry*, **41**, 5348–5358.
39. Ming, M., Lu, M., Balashov, S. P., Ebrey, T. G., Li, Q. & Ding, J. (2006). pH dependence of light-driven proton pumping by an archaerhodopsin from Tibet: comparison with bacteriorhodopsin. *Biophys. J.* **90**, 3322–3332.
40. Brown, L. S., Sasaki, J., Kandori, H., Maeda, A., Needleman, R. & Lanyi, J. K. (1995). Glutamic acid 204 is the terminal proton release group at the extracellular surface of bacteriorhodopsin. *J. Biol. Chem.* **270**, 27122–27126.
41. Balashov, S. P., Imasheva, E. S., Ebrey, T. G., Chen, N., Menick, D. R. & Crouch, R. K. (1997). Glutamate-194 to cysteine mutation inhibits fast light-induced proton release in bacteriorhodopsin. *Biochemistry*, **36**, 8671–8676.
42. Caffrey, M. & Cherezov, V. (2009). Crystallizing membrane proteins using lipidic mesophases. *Nat. Protoc.* **4**, 706–731.
43. Holm, L., Kaariainen, S., Rosenstrom, P. & Schenkel, A. (2008). Searching protein structure databases with DaliLite v.3. *Bioinformatics*, **24**, 2780–2781.
44. Neutze, R., Pebay-Peyroula, E., Edman, K., Royant, A., Navarro, J. & Landau, E. M. (2002). Bacteriorhodopsin: a high-resolution structural view of vectorial proton transport. *Biochim. Biophys. Acta*, **1565**, 144–167.
45. Shibata, M., Yamashita, H., Uchihashi, T., Kandori, H. & Ando, T. (2010). High-speed atomic force microscopy shows dynamic molecular processes in photoactivated bacteriorhodopsin. *Nat. Nanotechnol.* **5**, 208–212.
46. Wegener, A. A., Chizhov, I., Engelhard, M. & Steinhoff, H. J. (2000). Time-resolved detection of transient movement of helix F in spin-labelled *pharaonis* sensory rhodopsin II. *J. Mol. Biol.* **301**, 881–891.
47. Yoshida, H., Sudo, Y., Shimono, K., Iwamoto, M. & Kamo, N. (2004). Transient movement of helix F revealed by photo-induced inactivation by reaction of a bulky SH-reagent to cysteine-introduced *pharaonis* phoborhodopsin (sensory rhodopsin II). *Photochem. Photobiol. Sci.* **3**, 537–542.
48. Shimono, K., Ikeura, Y., Sudo, Y., Iwamoto, M. & Kamo, N. (2001). Environment around the chromophore in *pharaonis* phoborhodopsin: mutation analysis of the retinal binding site. *Biochim. Biophys. Acta*, **1515**, 92–100.
49. Shimono, K., Ikeura, Y., Sudo, Y., Iwamoto, M. & Kamo, N. (2002). Importance of the location of the negative-charged counter-ion against the protonated Schiff base on the chromophore configuration of *pharaonis* phoborhodopsin. *J. Photosci.* **9**, 302–304.
50. Shimono, K., Hayashi, T., Ikeura, Y., Sudo, Y., Iwamoto, M. & Kamo, N. (2003). Importance of the broad regional interaction for spectral tuning in *Natronobacterium pharaonis* phoborhodopsin (sensory rhodopsin II). *J. Biol. Chem.* **278**, 23882–23889.
51. Greenhalgh, D. A., Fareens, D. L., Subramaniam, S. & Khorana, H. G. (1993). Hydrophobic amino acids in the retinal-binding pocket of bacteriorhodopsin. *J. Biol. Chem.* **268**, 20305–20311.